Title
Synthesis and Characterization of 89Zr-Labeled Ultrasmall Nanoparticles

Journal
Molecular Pharmaceutics, 13(7)

ISSN
1543-8384

Authors
Truillet, Charles
Thomas, Eloise
Lux, Francois
et al.

Publication Date
2016-07-05

DOI
10.1021/acs.molpharmaceut.6b00264

Peer reviewed

Published in final edited form as:

Mol Pharm. 2016 July 05; 13(7): 2596–2601. doi:10.1021/acs.molpharmaceut.6b00264.

Synthesis and characterization of ^{89}Zr-labeled ultrasmall nanoparticles

Charles Truillet[1,†], **Eloise Thomas**[2,†], **Francois Lux**[2], **Loc T. Huynh**[1], **Olivier Tillement**[2], and **Michael J. Evans**[1,*]

[1]Department of Radiology and Biomedical Imaging, University of California San Francisco, 185 Berry Street, Lobby 6, Suite 350, San Francisco CA 94107,

[2]Institut Lumière Matière, UMR5306, Université Claude Bernard Lyon1-CNRS, Université de Lyon 69622 Villeurbanne cedex, France.

Abstract

The ultrasmall nanoparticle AGuIX is a versatile platform that tolerates a range of chemical diversity for theranostic applications. Our previous work showed that AGuIX clears rapidly from normal tissues, while durably accumulating within the tumor microenvironment. On this basis, AGuIX was used to detect tumor tissue with Gd^{3+} enhanced MRI, and can sensitize tumors to radiation therapy. As we begin the translation of AGuIX, we appreciated that coupling AGuIX to a long-lived radioisotope would help to more completely measure the magnitude and duration of its retention within the tumor microenvironment. Therefore, we developed ^{89}Zr-DFO-AGuIX. AGuIX was coupled to DFO and then to ^{89}Zr in ~99% radiochemical yield. Stability studies showed that ^{89}Zr-DFO-AGuIX did not dissociate after 72 hours. In animals bearing U87MG xenografts, it was detectable at levels above background for 72 hours. Lastly, ^{89}Zr-DFO-AGuIX did not accumulate in inflammatory abscesses *in vivo*, highlighting its specificity for well vascularized tumors.

Keywords

AGuIX; nanoparticle; Positron emission tomography; cancer

Introduction:

Owing to their chemical versatility and encouraging properties *in vivo*, nanotechnologies have been aggressively developed and refined over the past two decades for biomedical applications[1, 2]. We have previously developed AGuIX, an ultrasmall nanoparticle (NP) for theranostic applications in cancer[2–5]. AGuIX is ~10 kDa NP with a hydrodynamic diameter of ~3 nm. The core of the NP is a polysiloxane matrix, onto which chemically diverse chelators can be grafted. For instance, about 10 DOTAGA chelators have been engineered per NP to bind Gd^{3+} for contrast enhanced MRI *in vivo*[6, 7]. Moreover, alternative chelators can be attached onto AGuIX for nuclear imaging, and we recently engineered one additional NODAGA chelator to bind $^{68}Ga^{3+}$ to AGuIX for PET *in vivo*[8]. Lastly, near-infrared

*To whom the correspondence should be addressed: Michael J. Evans, michael.evans@ucsf.edu, phone: 415-353-3442.
†These authors contributed equally

fluorescent molecules can be conjugated to the NP to track its tissue localization with microscopy or to follow them by optical imaging[9, 10].

Applying these constructs *in vivo* to study the biodistribution of AGuIX longitudinally with MRI and PET has shown that the construct does not accumulate substantially in normal tissues, and rapidly clears from rodents via the kidneys. After 24 hours, ~90% of the NPs are cleared in the urine, with ~10% of the injected NPs bound within the kidneys and ~0.2% distributed in all other normal tissues. Microscopy with fluorescently tagged AGuIX showed retention within the proximal tubules of the kidneys, with subsequent excretion of the native or partially degraded NPs.[11]. Lastly, sufficient accumulation of the NP has been observed in the microenvironment of preclinical tumor models to amplify the therapeutic effects of external beam radiation therapy[11, 12,]. Collectively, these observations strongly justify first in man studies with AGuIX.

Long lived radioisotopes (*e.g.* zirconium-89, iodine-124) are essential to fully study the pharmacokinetics and biodistribution of molecules with higher order structure *in vivo*[13]. Because AGuIX can be readily engineered with chemically discrete chelators, we reasoned that ^{89}Zr could be incorporated onto chelates grafted at the surface of the polysiloxane core for nuclear imaging. Indeed, we and others have shown that ^{89}Zr is an excellent radionuclide to characterize monoclonal antibodies in preclinical models of cancer, and that ^{89}Zr can be stably coupled to large biomolecules with a desferrioxamine (DFO) chelator[13, 14]. These considerations motivated us to design a synthetic route to DFO-conjugated AGuIX, and to evaluate the properties of ^{89}Zr-DFO-AGuIX *in vitro* and *in vivo*.

Experimental Section:

Chemicals:

Sodium hydroxide (NaOH, 99.99%), hydrochloric acid (HCl, 36.5−38%) and dimethylsulfoxide (DMSO, >99.5%) were purchased from Aldrich Chemical (France), acetonitrile (CH3CN, >99.9%) was purchased from Carlo Erba (France), trifluoroacetic acid (TFA, >99%) was purchased from Alfa Aesar (United Kingdom), copper sulfate pentahydrate ($CuSO_4.5H_2O$, 98%) was purchased from Merck (Germany). AGuIX particles were purchased from Nano-H (Saint-Quentin Fallavier, France). The desferrioxamine chelate, p-NCS-Bz-DFO (N1-hydroxy-N1-(5-(4-(hydroxy(5-(3-(4-isothiocyanatophenyl)thioureido)pentyl)amino)-4-oxobutanamido)pentyl)-N4-(5-(N-hydroxyacetamido)pentyl)succinamide) was purchased from ChemaTech (France). All products were used without further purification. Only Mili-Q water (ρ>18MΩ.cm) was used for the aqueous solution preparation.

Synthesis of DFO-AGuIX:

AGuIX nanoparticles (500 μmol based on $[Gd^{3+}]$, 1 eq.) were dispersed in 6.67 mL of water for 1 hour at a pH of 7.4. 37.6 mg of p-NCS-Bz-DFO (50 μmol, 1 eq.) were dissolved in 4.80 mL of DMSO. The DMSO solution was then gradually added over 8 hours to the AGuIX solution under stirring at 50°C. The addition was performed gradually to prevent precipitation of the ligands and of the functionalized product. After addition was complete,

the pH was decreased to 5.0 with 1M HCl solution and stirred at room temperature overnight to precipitate free unreacted DFO. Unreacted DFO was firstly removed by centrifugation; all other other unreacted products were removed by tangential filtration trough Vivaspin® membranes (molecular weight threshold = 5 kDa, Sartorius Stedim Biotech). The DFO-AGuIX solution was concentrated to approximately [Gd^{3+}] = 100 mM after many cycles of tangential filtration. The solution was sterile filtered through 0.2 μm syringe filter in order to remove the largest impurities. It was then freeze-dried for storage, using a Christ Alpha 1–2 lyophilizer. The Gd^{3+} yield for the synthesis of AGuIX prior to conjugating to DFO was 48%, which was determined with relaxometry and inductively coupled plasma mass spectrometry as reported previously[8]. After conjugation of DFO to AGuIX, the yield of the final molecule was determined to be 68% using ICP-MS.

Radiochemistry:

To a solution of [^{89}Zr]Zr-oxalic acid (1.2mCi; 12 μl) and 2 M Na_2CO_3 (12 μl) was added 0.30 ml of 0.5 M HEPES (pH 7.1–7.3), 0.50 ml of DFO-AGuIX (pH = 7, 22.5 μmoles Gd) or 0.50 of DFO (Deferoxamine mesylate salt, pH = 7, 15 mg), and 0.70 ml 0.5 M HEPES (pH 7.1–7.3) into the reaction vial were added. After incubation (120 minutes) at 37° C, the radiolabeling yield was determined by iTLC. The final product was filtered through a 0.2 micron filter into a sterile vial. Radiolabeling efficiency (typically > 98.5%) was determined by ITLC using chromatography strips and 20 mM citric acid (pH 4.9–5.1) as the mobile phase. *In vitro* stability of ^{89}Zr-AGuIX was assessed in serum for up to 3 days. For the serum stability studies, 50 μL ^{89}Zr-AGuIX at 50 mM in Gd^{3+} were added to 450 μL serum and the mixture was incubated at 37 °C. Samples were taken at 1h, 4h, 24h, and 75h and assessed by ITLC. ^{89}Zr-transferrin was prepared as previously described[15].

Serum stability determination:

Blood samples were immediately subjected to centrifugation at 2300g for 15 min at 4 °C, and the serum supernatants were collected. The supernatant was immediately aliquoted and studied. *In vitro*, 50 μCi ^{89}Zr-DFO-AGuIX were incubated with 100% fetal bovine serum and aliquots were reserved for analysis at 1 hr, 4 hr, 8 hr, 24 hr and 72 hr. Healthy *nu/nu* mice (8–10 weeks old, n = 3) were injected with 50 ± 3 uCi of ^{89}Zr-DFO-AGuIX preparation in 100 μL HEPES solution (pH=7.4). Blood was sampled from the submandibular vein at 1 hr, 4 hr, 8 hr, 24 hr and 72 hr post injection. Activity within the blood samples was resolved by ITLC and each experiment was carried out in triplicate.

Animal studies:

All animal protocols were approved by the UCSF Administrative on Laboratory Animal Care. For tumor imaging studies, 8-wk-old male nude (nu/nu) mice (Charles River Laboratories) were injected subcutaneously with 1×10^6 cells containing 50% Matrigel (v/v) in the flank while anesthetized with 2% isoflurane. Animals were used for imaging studies with MRI and PET once the tumors became palpable. For MRI studies, AGuIX (20 μmol) and DOTAREM (20 μmol) were administered via tail vein injection. Animals were imaged with MRI 20 minutes post injection. For biodistribution studies with inflammatory abscesses, ~50 μL of turpentine oil (Sigma Aldrich) was injected subcutaneously in the right hind limb per a previously established methodology[16]. Fifteen minutes was allowed to pass

to generate the acute phase response, whereupon the mice were injected with ^{89}Zr-transferrin or ^{89}Zr-DFO-AGuIX. Animals were euthanized 30 min post injection with CO_2 (g) asphyxiation.

Magnetic resonance imaging:

All MRI acquisitions were performed on a 7T Small Animal MRI facility at UCSF, using a 7T 300 MHz Horizontal Bore Varian MR System. Pre and Post-treatment MR imaging was performed. A multislice spin-echo sequence was used to generate spin-density weighted images, with a TR of 3000 ms and a TE of 18 ms. Sample scans had an acquisition matrix of 128×128 points, with the field of view measuring 19.2×19.2 mm. Prior to injection in mice, a concentrated colloid (AGuIX in water, [Gd^{3+}] = 100 mM) was diluted by saline solution in order to obtain an intravenous use solution ([Gd^{3+}] = 50 mM). The pH was adjusted to 7.4. Before use, this solution was filtered onto syringe filter with nylon membrane (pore diameter 0.22 μm). The chelate used was DOTAREM® (laboratories Guerbet, Aulnay sous Bois France, 0.5 mM/mL) as available in MRI units. The aqueous AGuIX was manually injected in the tail vein at 200 μL volume. The gadolinium chelates were injected via the tail vein at the same concentration (50mM) at 200 μL volume.

Results:

AGuIX NPs were synthesized according to our previously established, top-down protocol. Briefly, gadolinium oxide cores were first synthesized in diethylene glycol. The oxide core was coated with a polysiloxane shell using hydrolysis–condensation of aminopropyl triethoxysilane (APTES) and tetraethyl orthosilicate (TEOS). DOTAGA groups (1,4,7,10-tetra-azacyclododecane-1-glutaric anhydride-4,7,10-triacetic acid) were then covalently ligated onto the nanoparticles via a primary amine from APTES. To induce core dissolution, the NPs were transferred from DEG to water. The resulting polysiloxane hollow cores were collapsed and fragmented into small and rigid platforms of polysiloxane. The resulting NPs bear on their surface DOTAGA molecules that are chelated to Gd^{3+} cations.[7]

To prepare DFO-AGuIX, 1-(4-isothiocyanatophenyl)-3- [6,17-dihydroxy-7,10,18,21-tetraoxo-27-(N-acetylhydroxylamino)-6,11,17,22-tetraazaheptaeicosine] thiourea (p-NCS-Bz-DFO) was incubated with AGuIX for one hour at room temperature. DFO was covalently ligated to the solvent exposed primary amines contained within APTES, and the resulting functional group was a thiourea. DFO-AGuIX was subjected to tangential filtration over a 5 kDa membrane to remove any unconjugated p-NCS-Bz-DFO at pH 5. DFO-AGuIX NPs were then freeze−dried for storage.

We expected that adding DFO to AGuIX would change its retention on reverse phase HPLC. On this basis, we subjected DFO-AGuIX to RP-HPLC to determine its purity. Naked AGuIX, DFO-AGuIX, and free DFO were loaded into the injection loop separately. The corresponding chromatogram from the DFO-AGuIX showed peaks at 2.5 min corresponding to degradation fragments of DFO-AGuIX due to the hydrolysis of silyl ether bonds in diluted medium[17]. The major peak at 13–14 min corresponded to DFO-AGuIX (Figure 1A). Moreover, DFO-AGuIX eluted later than AGuIX and no free DFO was detected in the DFO-AGuIX formulation. The final colloidal solution was characterized by dynamic light

scattering and DFO-AGuIX was determined to have a hydrodynamic diameter of 4.4 ± 1 nm (slightly larger to the hydrodynamic diameter of naked AGuIX that is 3.6 ± 0.8 nm, Figure 1B), which is suitable for renal excretion.

To quantify the number of DFO molecules per AGuIX, we titrated Cu^{2+} into a preparation of DFO-AGuIX ($[Gd^{3+}]$ = 38.4 mM) and resolved the free and AGuIX bound Cu^{2+} with HPLC. We chose to utilize Cu^{2+} for several reasons. First, the constant of complexation between Cu^{2+} and DFO has been calculated[18], and is only two fold less than Fe^{3+} ($\log \beta$ = 23.98 for $[CuLH]^0$, $\log \beta$ = 41.01 for $[FeLH]^+$). Moreover, Cu(II) sulfate is easily detected at 700 nm. Lastly, we have previously developed, validated and published this HPLC based approach using Cu(II) sulfate to determine the number of NODA chelators on the AGuIX scaffold[8].

On titration, a free fraction of Cu(II) sulfate was initially detected at ~7 mM of Cu^{2+}, and this point of inflection allowed us to estimate between 1–2 DFO chelators per DFO-AGuIX (Figure 1C and Supplemental Figure 1). A detectable but negligible amount of unknown Cu(II) conjugated degradation products were also observed (Supplemental Figure 2). These early eluting peaks did not interfere with the integration of the Cu(II) sulfate peak on the HPLC trace. ICP-MS performed on DFO-AGuIX also resulted in a relative composition consistent with 1–2 DFO molecules per AGuIX: $Gd_{10}APTES^*_{27.8}TEOS^*_{26.6}DOTAGA^*_{10.2}DFO^*_{1.4}$. Lastly, a separate set of experiments with Cu^{2+} and naked AGuIX lacking DFO showed almost no evidence of binding (Supplemental Figure 3). This indicates that the DOTAGA chelators within AGuIX are saturated with Gd^{3+} (free chelate < 2%), and the Cu^{2+} binding observed with DFO-AGuIX is due to an interaction between Cu^{2+} and DFO.

DFO-AGuIX was then metallated with ^{89}Zr-oxalate in one hour to a radiochemical yield of 99%. Unreacted ^{89}Zr-oxalate was removed by centrifugal membrane filtration per a previous protocol[19]. The radiochemical purity was determined to be 100% by iTLC using 20 mM citric acid as the mobile phase (Figure 2A and Supplemental Figure 4).

We next evaluated the stability of ^{89}Zr-DFO-AGuIX *in vitro* and *in vivo*. No detectable degradation of ^{89}Zr-DFO-AGuIX was observed after 72 hours of incubation at 37° C in bovine serum (Figure 2B). Moreover, no evidence of degradation was observed in the serum harvested from mice injected intravenously with ^{89}Zr-DFO-AGuIX (Figure 2C and Supplemental Figure 5). Because ^{89}Zr-DFO-AGuIX was very stable, we determined the biological half-life of the construct in normal mice. Serial measurements of total activity in tumor naïve *nu/nu* mice injected with ^{89}Zr-AGuIX intravenously showed that the biological half-life is ~ 67 hours (Supplemental Figure 6).

We next asked if ^{89}Zr-DFO-AGuIX accumulates within a subcutaneous tumor model in mice. Male *nu/nu* mice inoculated with subcutaneous U87MG tumors were injected with ^{89}Zr-DFO-AGuIX intravenously, and the biodistribution was monitored over time. After observing evidence of accumulation in the tumor with MRI 20 min post injection due to the positive contrast agent properties of DFO-AGuIX (r_1 = 16.7 $mmol^{-1}.s^{-1}$ and r_2/r_1 = 1.5 at 37°C and 1.4 T) (Supplemental Figure 7), we investigated the tumor associated activity from

24 – 72 hours with biodistribution studies. Durable retention of the NPs (~2% ID/g) was observed in human glioma U87MG tumors, and was statistically greater than the accumulation of ^{89}Zr-DFO (~0.5% ID/g at 24 hours post injection, see Figure 3A and 3B, and Supplemental Figures 8 and 9 for biodistribution from a larger panel of normal tissues.). The tumor to blood and tumor to muscle ratio for ^{89}Zr-AGuIX incrementally increased over time to values greater than 10 at 72 hours post injection (Figure 3C). The uptake in other normal tissues was low, as expected, with the notable exception of the kidneys (Supplemental Figure 9). Autoradiography of the tumor slices *ex vivo* also showed that the highest degree of activity within the tumor slices co-localized with areas harboring visually obvious pericellular compartments (Supplemental Figure 10). Lastly, we tested whether ^{89}Zr-DFO-AGuIX accumulated in inflammatory abscesses *in vivo*. After inducing an acute phase response with an intramuscular injection of turpentine, normal *nu/nu* mice were treated with ^{89}Zr-DFO-AGuIX or ^{89}Zr-transferrin, a molecule we previously showed to localize to sites of inflammation[15]. After 30 min, a biodistribution study was conducted to determine the amount of activity in the inflamed muscle and normal tissues. The uptake of ^{89}Zr-Tf was higher in the inflamed muscle compared to the untreated contralateral muscle, as expected. However, no difference in activity was observed between the inflamed and untreated muscles of mice treated with ^{89}Zr-AGuIX (Figure 3D and Supplemental Figure 11). Moreover, the level of tissue associated activity in the inflamed muscle was ~0.5% ID/g, or roughly equal to what was observed for ^{89}Zr-DFO in U87MG tumors.

Discussion:

In this report, we describe the synthesis and characterization of AGuIX functionalized with DFO, and conjugated to ^{89}Zr. The construct was synthesized from AGuIX in two steps to >98% radiochemical yield. Consistent with our expectations, the radiolabeled construct is stable out to 72 hours *in vitro* and *in vivo*, and durably accumulates into subcutaneous tumors during this time period. Finally, ^{89}Zr-DFO-AGuIX did not accumulate in inflammatory abscesses *in vivo*, as expected. Collectively, these data support the use of ^{89}Zr-DFO-AGuIX as a tool to measure the biodistribution and pharmacokinetics of AGuIX in a first-in-man study.

To our knowledge, this is the first example of a ^{89}Zr-labeled ultrasmall nanoparticle, though others have conjugated ^{89}Zr to larger nanoparticles with longer circulation times[20–24]. As we demonstrate, the use of ^{89}Zr is justified, as AGuIX can persist for days in the tumor microenvironment due to the enhanced permeability and retention effect. Consistent with previous MR and microscopy data, accumulation within the kidney also persists for days, extending the biological half-life of AGuIX[25]. Moreover, we felt a radiometal-based approach (as opposed to a halogen) was appropriate, as we have previously shown that chemically discrete chelators can be added to the polysiloxane core after functionalization with DOTAGA and saturation with Gd^{3+}. Lastly, ^{89}Zr was an attractive radionuclide to work with, owing to its long half-life (~78 hours), and the recently clinical data showing it is well tolerated in patients when attached to monoclonal antibodies[26, 27].

Incorporating a long lived radioisotope for PET onto AGuIX presents a more realistic approach to quantify the amount of NPs in cancer at later time points post injection. While

our preclinical experience with AGuIX shows that its concentration in tumors can be calculated with MRI within minutes to hours post injection, contrast becomes more difficult to detect in tumors >24 hours post injection[4]. By comparison, a ~1 hour PET acquisition should be sufficient to acquire the ~10 million coincident events needed for tumor contrast based on the magnitude of radioactivity detected in the biodistribution study. PET also broadens the dynamic range of concentrations that can be measured by lowering the limit of NP detection compared to contrast enhanced MRI. All of these considerations are significant, as the pharmacokinetics of the NP will dictate the design of a pending clinical trial to determine its value as a radiosensitizer.

Using our current synthetic scheme, approximately 1 molecule of DFO was incorporated per AGuIX NP. In the future, we anticipate more DFO chelators can be added to the unreacted primary amines on the polysiloxane core, which in turn could favorably raise the specific activity of the construct. Along these lines, our data also argues strongly for the ligation of ^{89}Zr-AGuIX onto large biomolecules (*e.g.* IgG, Fab) for immunoPET applications[14]. We are currently exploring these frontiers.

Supplementary Material

Refer to Web version on PubMed Central for supplementary material.

Acknowledgements:

The authors acknowledge Sergio Wong, and Drs Youngho Seo and Sergey Magnitsky for assistance with the biodistribution studies and MRI experiments, and Frederic Boschetti from CheMatech SAS for the furnishing of p-NCS-Bz-DFO. M.J.E., C.T., and L.T.H. were supported by the 2013 David H. Koch Young Investigator Award from the Prostate Cancer Foundation, by the National Institutes of Health (R00CA172695, 1R01CA17661-01), and the Department of Defense Prostate Cancer Research Program (PC140107, PC151060). E.T., F.L. and O.T. were supported by the French National Research Agency (ANR6126RPIB-0010 Multimage).

References:

1. Hainfeld JF; Smilowitz HM; O'Connor MJ; Dilmanian FA; Slatkin DN Gold nanoparticle imaging and radiotherapy of brain tumors in mice. Nanomedicine 2013, 8, (10), 1601–9. [PubMed: 23265347]
2. Lux F; Mignot A; Mowat P; Louis C; Dufort S; Bernhard C; Denat F; Boschetti F; Brunet C; Antoine R; Dugourd P; Laurent S; Vander Elst L; Muller R; Sancey L; Josserand V; Coll JL; Stupar V; Barbier E; Remy C; Broisat A; Ghezzi C; Le Duc G; Roux S; Perriat P; Tillement O Ultrasmall rigid particles as multimodal probes for medical applications. Angewandte Chemie 2011, 50, (51), 12299–303. [PubMed: 22057640]
3. Sancey L; Lux F; Kotb S; Roux S; Dufort S; Bianchi A; Cremillieux Y; Fries P; Coll JL; Rodriguez-Lafrasse C; Janier M; Dutreix M; Barberi-Heyob M; Boschetti F; Denat F; Louis C; Porcel E; Lacombe S; Le Duc G; Deutsch E; Perfettini JL; Detappe A; Verry C; Berbeco R; Butterworth KT; McMahon SJ; Prise KM; Perriat P; Tillement O The use of theranostic gadolinium-based nanoprobes to improve radiotherapy efficacy. The British journal of radiology 2014, 87, (1041), 20140134. [PubMed: 24990037]
4. Le Duc G; Roux S; Paruta-Tuarez A; Dufort S; Brauer E; Marais A; Truillet C; Sancey L; Perriat P; Lux F; Tillement O Advantages of gadolinium based ultrasmall nanoparticles vs molecular gadolinium chelates for radiotherapy guided by MRI for glioma treatment. Cancer nanotechnology 2014, 5, (1), 4. [PubMed: 26561512]

5. Detappe A; Kunjachan S; Rottmann J; Robar J; Tsiamas P; Korideck H; Tillement O; Berbeco R AGuIX nanoparticles as a promising platform for image-guided radiation therapy. Cancer nanotechnology 2015, 6, (1), 4. [PubMed: 26345984]
6. Bianchi A; Dufort S; Fortin PY; Lux F; Raffard G; Tassali N; Tillement O; Coll JL; Cremillieux Y In vivo MRI for effective non-invasive detection and follow-up of an orthotopic mouse model of lung cancer. NMR in biomedicine 2014, 27, (8), 971–9. [PubMed: 24913958]
7. Mignot A; Truillet C; Lux F; Sancey L; Louis C; Denat F; Boschetti F; Bocher L; Gloter A; Stephan O; Antoine R; Dugourd P; Luneau D; Novitchi G; Figueiredo LC; de Morais PC; Bonneviot L; Albela B; Ribot F; Van Lokeren L; Dechamps-Olivier I; Chuburu F; Lemercier G; Villiers C; Marche PN; Le Duc G; Roux S; Tillement O; Perriat P A top-down synthesis route to ultrasmall multifunctional Gd-based silica nanoparticles for theranostic applications. Chemistry 2013, 19, (19), 6122–36. [PubMed: 23512788]
8. Truillet C; Bouziotis P; Tsoukalas C; Brugiere J; Martini M; Sancey L; Brichart T; Denat F; Boschetti F; Darbost U; Bonnamour I; Stellas D; Anagnostopoulos CD; Koutoulidis V; Moulopoulos LA; Perriat P; Lux F; Tillement O Ultrasmall particles for Gd-MRI and (68) Ga-PET dual imaging. Contrast media & molecular imaging 2015, 10, (4), 309–19. [PubMed: 25483609]
9. Morlieras J; Dufort S; Sancey L; Truillet C; Mignot A; Rossetti F; Dentamaro M; Laurent S; Vander Elst L; Muller RN; Antoine R; Dugourd P; Roux S; Perriat P; Lux F; Coll JL; Tillement O Functionalization of small rigid platforms with cyclic RGD peptides for targeting tumors overexpressing alphavbeta3-integrins. Bioconjugate chemistry 2013, 24, (9), 1584–97. [PubMed: 23978076]
10. Morlieras J; Chezal JM; Miot-Noirault E; Roux A; Heinrich-Balard L; Cohen R; Tarrit S; Truillet C; Mignot A; Hachani R; Kryza D; Antoine R; Dugourd P; Perriat P; Janier M; Sancey L; Lux F; Tillement O Development of gadolinium based nanoparticles having an affinity towards melanin. Nanoscale 2013, 5, (4), 1603–15. [PubMed: 23334308]
11. Lux F; Sancey L; Bianchi A; Cremillieux Y; Roux S; Tillement O Gadolinium-based nanoparticles for theranostic MRI-radiosensitization. Nanomedicine 2015, 10, (11), 1801–15. [PubMed: 25715316]
12. Le Duc G; Miladi I; Alric C; Mowat P; Brauer-Krisch E; Bouchet A; Khalil E; Billotey C; Janier M; Lux F; Epicier T; Perriat P; Roux S; Tillement O Toward an image-guided microbeam radiation therapy using gadolinium-based nanoparticles. ACS nano 2011, 5, (12), 9566–74. [PubMed: 22040385]
13. Zeglis BM; Houghton JL; Evans MJ; Viola-Villegas N; Lewis JS Underscoring the influence of inorganic chemistry on nuclear imaging with radiometals. Inorganic chemistry 2014, 53, (4), 1880–99. [PubMed: 24313747]
14. Evans MJ Measuring oncogenic signaling pathways in cancer with PET: an emerging paradigm from studies in castration-resistant prostate cancer. Cancer discovery 2012, 2, (11), 985–94. [PubMed: 23043150]
15. Holland JP; Evans MJ; Rice SL; Wongvipat J; Sawyers CL; Lewis JS Annotating MYC status with 89Zr-transferrin imaging. Nature medicine 2012, 18, (10), 1586–91.
16. Jennings G; Elia M The acute-phase response to turpentine-induced abscesses in malnourished rats at different environmental temperatures. Metabolism: clinical and experimental 1992, 41, (2), 141–7. [PubMed: 1370974]
17. Truillet C; Lux F; Tillement O; Dugourd P; Antoine R Coupling of HPLC with electrospray ionization mass spectrometry for studying the aging of ultrasmall multifunctional gadolinium-based silica nanoparticles. Analytical chemistry 2013, 85, (21), 10440–7. [PubMed: 24160370]
18. Crisponi G; Nurchi VM; Crespo-Alonso M; Sanna G; Zoroddu MA; Alberti G; Biesuz R A Speciation Study on the Perturbing Effects of Iron Chelators on the Homeostasis of Essential Metal Ions. PloS one 2015, 10, (7), e0133050. [PubMed: 26192307]
19. Vosjan MJ; Perk LR; Visser GW; Budde M; Jurek P; Kiefer GE; van Dongen GA Conjugation and radiolabeling of monoclonal antibodies with zirconium-89 for PET imaging using the bifunctional chelate p-isothiocyanatobenzyl-desferrioxamine. Nature protocols 2010, 5, (4), 739–43. [PubMed: 20360768]

20. Keliher EJ; Yoo J; Nahrendorf M; Lewis JS; Marinelli B; Newton A; Pittet MJ; Weissleder R 89Zr-labeled dextran nanoparticles allow in vivo macrophage imaging. Bioconjugate chemistry 2011, 22, (12), 2383–9. [PubMed: 22035047]

21. Chen F; Goel S; Valdovinos HF; Luo H; Hernandez R; Barnhart TE; Cai W In Vivo Integrity and Biological Fate of Chelator-Free Zirconium-89-Labeled Mesoporous Silica Nanoparticles. ACS nano 2015, 9, (8), 7950–9. [PubMed: 26213260]

22. Miller L; Winter G; Baur B; Witulla B; Solbach C; Reske S; Linden M Synthesis, characterization, and biodistribution of multiple 89Zr-labeled pore-expanded mesoporous silica nanoparticles for PET. Nanoscale 2014, 6, (9), 4928–35. [PubMed: 24675844]

23. Perez-Medina C; Abdel-Atti D; Zhang Y; Longo VA; Irwin CP; Binderup T; Ruiz-Cabello J; Fayad ZA; Lewis JS; Mulder WJ; Reiner T A modular labeling strategy for in vivo PET and near-infrared fluorescence imaging of nanoparticle tumor targeting. Journal of nuclear medicine : official publication, Society of Nuclear Medicine 2014, 55, (10), 1706–11.

24. Perez-Medina C; Tang J; Abdel-Atti D; Hogstad B; Merad M; Fisher EA; Fayad ZA; Lewis JS; Mulder WJ; Reiner T PET Imaging of Tumor-Associated Macrophages with 89Zr-Labeled High-Density Lipoprotein Nanoparticles. Journal of nuclear medicine : official publication, Society of Nuclear Medicine 2015, 56, (8), 1272–7.

25. Sancey L; Kotb S; Truillet C; Appaix F; Marais A; Thomas E; van der Sanden B; Klein JP; Laurent B; Cottier M; Antoine R; Dugourd P; Panczer G; Lux F; Perriat P; Motto-Ros V; Tillement O Long-term in vivo clearance of gadolinium-based AGuIX nanoparticles and their biocompatibility after systemic injection. ACS nano 2015, 9, (3), 2477–88. [PubMed: 25703068]

26. Pandit-Taskar N; O'Donoghue JA; Durack JC; Lyashchenko SK; Cheal SM; Beylergil V; Lefkowitz RA; Carrasquillo JA; Martinez DF; Fung AM; Solomon SB; Gonen M; Heller G; Loda M; Nanus DM; Tagawa ST; Feldman JL; Osborne JR; Lewis JS; Reuter VE; Weber WA; Bander NH; Scher HI; Larson SM; Morris MJ A Phase I/II Study for Analytic Validation of 89Zr-J591 ImmunoPET as a Molecular Imaging Agent for Metastatic Prostate Cancer. Clinical cancer research : an official journal of the American Association for Cancer Research 2015, 21, (23), 5277–85. [PubMed: 26175541]

27. Dijkers EC; Oude Munnink TH; Kosterink JG; Brouwers AH; Jager PL; de Jong JR; van Dongen GA; Schroder CP; Lub-de Hooge MN; de Vries EG Biodistribution of 89Zr-trastuzumab and PET imaging of HER2-positive lesions in patients with metastatic breast cancer. Clinical pharmacology and therapeutics 2010, 87, (5), 586–92. [PubMed: 20357763]

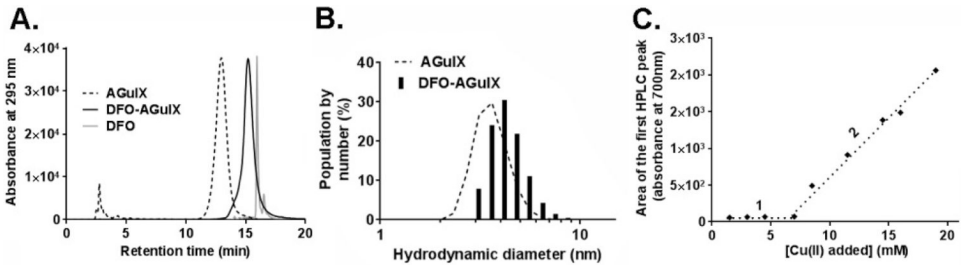

Figure 1.

Synthesis and characterization of DFO-AGuIX. A. An overlay of reverse phase HPLC traces showing the resolution of DFO-AGuIX at ~15 min compared to naked AGuIX (~13 min) and free DFO (~16 min). These data also underscore the purity of DFO-AGuIX after filtration. The early eluting peaks on the AGuIX HPLC trace are minor degradation products. They do not appear on the DFO-AGuIX trace because they are removed with reaction purification. B. Dynamic light scattering data showing that the hydrodynamic diameter of DFO-AGuIX is larger than naked AGuIX, as expected. These data were acquired using the purified DFO-AGuIX material. C. Determination of the number of DFO chelates per AGuIX nanoparticle using Cu^{2+} titration and UV/Vis spectroscopy. The area under the peak corresponding to free Cu^{2+} was calculated after addition of Cu^{2+} on DFO-AGuIX and injection in HPLC (see also Supplemental Figure 1). Under sub-saturating conditions (1), no peak was detected, while increasing the concentration of Cu^{2+}, free Cu^{2+} ions were detected as the concentration exceeded ~7 mM (2). This assay was conducted with 38.4 mM AGuIX (in $[Gd^{3+}]$).

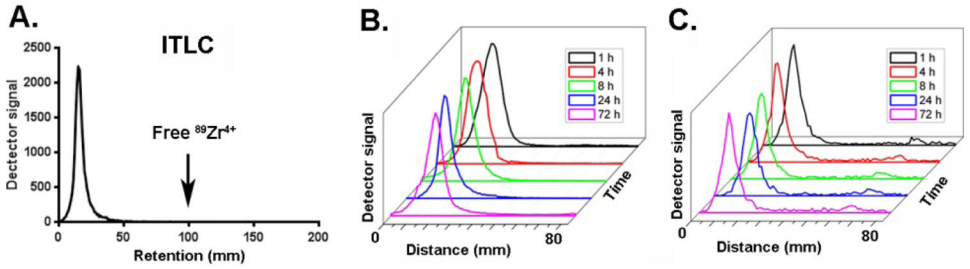

Figure 2.

Synthesis and characterization of ^{89}Zr-DFO-AGuIX. A. A representative ITLC showing the near complete metallation of DFO-AGuIX with ^{89}Zr-oxalate. The large peak corresponds to activity at the baseline, interpreted to be ^{89}Zr-AGuIX, and an arrow indicates the expected R_f for ^{89}Zr-oxalate (see also Supplemental Figure 5). B. Representative ITLC traces showing the stability of ^{89}Zr-DFO-AGuIX over time in neat fetal bovine serum. No peaks were resolved from baseline, suggesting that ^{89}Zr-DFO-AGuIX is not metabolized to smaller radioactive byproducts. C. Representative iTLC traces showing the stability of ^{89}Zr-DFO-AGuIX over time in in mouse serum. Mice were injected with ~50 μCi of ^{89}Zr-DFO-AGuIX, and blood was harvested at the indicated time point. The isolated serum was spotted and resolved by iTLC.

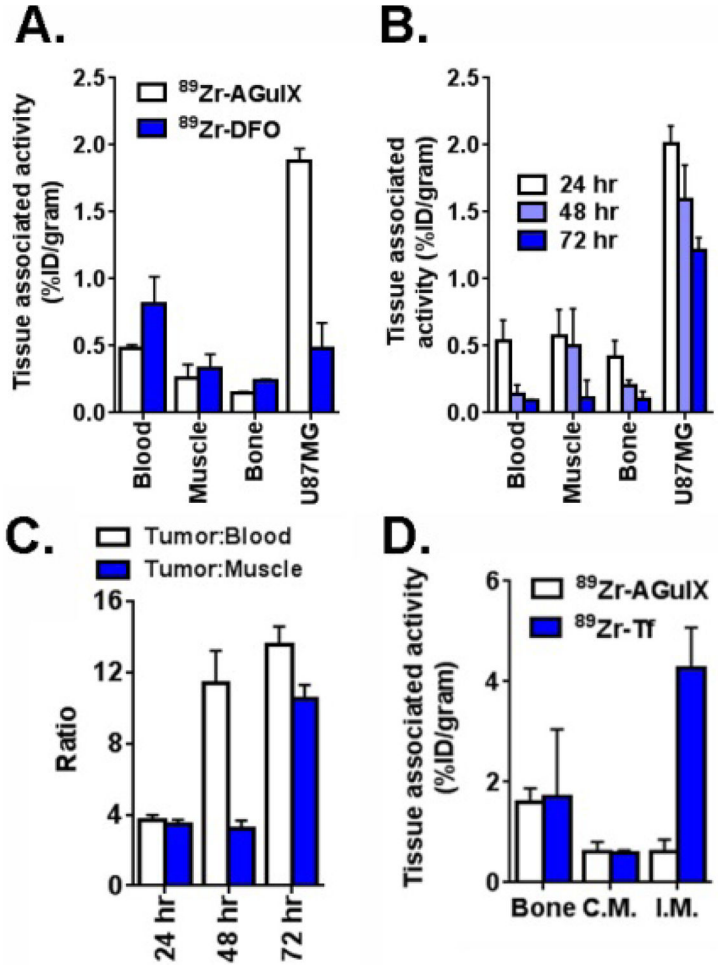

Figure 3.

^{89}Zr-DFO-AGuIX accumulates in the tumor microenvironment, but not in inflammatory abscesses. A. Biodistribution data at 24 hours post injection of ^{89}Zr-DFO-AGuIX or ^{89}Zr-DFO shows significantly higher uptake of the NP in the microenvironment of subcutaneous U87MG tumors compared to ^{89}Zr-DFO. No substantial differences were observed in muscle or bone, two normal reference tissues, from the cohorts receiving either radionuclide. B. Biodistribution data showing that ^{89}Zr-DFO-AGuIX persists in the tumor microenvironment for several days post injection. At 72 hours, the tumor associated activity was ~1.0% ID/g, which is above background. C. A graphical representation of the mean tumor to muscle and tumor to blood ratios over time for mice treated with ^{89}Zr-DFO-AGuIX. D. Biodistribution data showing no uptake of ^{89}Zr-DFO-AGuIX in the inflamed muscles within the hindlimbs of a mouse cohort. By comparison, ^{89}Zr-transferrin showed robust uptake in the inflamed muscle, presumably owing to the abundant expression of the transferrin receptor on peripheral mononuclear blood cells. I.M. = inflamed muscle, C.M. = contralateral unmanipulated muscle.